Multi Input Dynamical Modeling of Heat Flow With Uncertain Diffusivity Parameter

Mehmet Önder Efe & HItay Özbay

Taylor & Francis
Taylor & Francis Group

Multi Input Dynamical Modeling of Heat Flow With Uncertain Diffusivity Parameter

MEHMET ÖNDER EFE[1] AND HİTAY ÖZBAY[2]

ABSTRACT

This paper focuses on the multi-input dynamical modeling of one-dimensional heat conduction process with uncertainty on thermal diffusivity parameter. Singular value decomposition is used to extract the most significant modes. The results of the spatiotemporal decomposition have been used in cooperation with Galerkin projection to obtain the set of ordinary differential equations, the solution of which synthesizes the temporal variables. The spatial properties have been generalized through a series of test cases and a low order model has been obtained. Since the value of the thermal diffusivity parameter is not known perfectly, the obtained model contains uncertainty. The paper describes how the uncertainty is modeled and how the boundary conditions are separated from the remaining terms of the dynamical equations. The results have been compared with those obtained through analytic solution.

Keywords: Heat Conduction, multi-input modeling, singular value decomposition, model reduction, infinite dimensional system.

1. INTRODUCTION

Modeling of systems displaying spatial continuum requires a careful consideration since the physical process under investigation is of infinite dimensions. Efforts in understanding the behavior of such systems have particularly focused on the low dimensional models capturing the essential behavioral properties with a few Ordinary Differential Equations (ODEs). This has been done by using modal decompositions such as Proper Orthogonal Decomposition (POD) and Singular Value Decomposition (SVD). Although neither the decomposition techniques nor the infinite dimensionality are new issues in this field, obtaining a model having the boundary conditions as external inputs is a major problem in the POD and SVD methods. More explicitly, these approaches result in models where external control input appears in the

---

[1]Address correspondence to: Mehmet Önder Efe, Mechatronics Engineering Department, Atilim University, İncek, Gölbaşı, TR-06836 Ankara, Turkey.
[2]Department of Electrical and Electronics Engineering, Bilkent University, Bilkent, Ankara, TR-06800, Turkey; on leave from Collaborative Center of Control Science, Electrical Engineering Department, The Ohio State University, Columbus, OH 43210, USA.

dynamical equations implicitly, and this is not very useful for controller design. Another difficulty is the presence of modeling uncertainties, which stem from varying internal parameters or hypotheses that are not thoroughly valid. For the heat conduction process, imprecise knowledge on thermal diffusivity parameter is a good example to study uncertainties.

The use of decomposition techniques in modeling of spatially continuous systems has extensively been studied in the field of aerodynamic flow control problems, [1–4]. Since the dynamics of the process under investigation is governed by Navier–Stokes equations, obtaining closed form solutions are very difficult and the modeling studies particularly focus on the real time observations from the process. For systems having two or more spatial dimensions, the POD technique has been utilized with the aid of snapshots method, [1, 2]. Alternatively, for single dimensional processes, the same modeling procedure can be followed by exploiting the SVD technique.

Procedurally, in both of them, if the numerical data contains coherent modes, the expansion accurately describes the temporal modes and the spatial components distributing them over the physical domain of the process. Furthermore, the ortho-normality of the basis functions, which describe the spatial properties, helps in finding a set of ODEs synthesizing the temporal modes. Although the algorithmic part seems straightforward, the final form of the ODEs depicts an autonomous system having no external input. At this point, several modifications are needed to separate the effect of boundary conditions, which constitute the inputs exciting the process. Single dimensional heat conduction problem is therefore a good candidate to study how such modeling issues are addressed.

A number of variations of this problem has been taken into consideration in former studies, [5–7]. Atwell and King [5, 6], have considered two-dimensional heat conduction problem with control input explicitly available in the PDE. The thermal diffusivity parameter has been taken as a known constant and several control strategies have been assessed with the modeling results of POD approach. In [6], the design has been discussed from the computational point of view.

Another work focusing on one-dimensional heat conduction problem reports the design of time-optimal boundary control, [7]. It is emphasized in [7] that the time-optimal control has the bang-bang property, and the solution has been postulated by the techniques of Hilbert spaces. Rösch [8], views the characterization of boundary condition as an identification problem, and presents an iterative approach to meet the conditions of optimality.

Although the techniques of functional analysis suggest several solutions to the problem at hand [9], the technique presented in this paper can be generalized to a variety of systems displaying arbitrarily complicated behavior. This is intimately related to the fact that the approach is observation-based, that is, the dynamical content of the resulting model is confined to what is implied in the data leading to the model. In [10, 11], we demonstrate the modeling and control issues on 1D Burgers

equation and 2D heat equation. The results presented in [11] are particularly important in the sense that the parameters of the dynamic model changes if the frequency content of the boundary conditions changes. In other words, every model is valid only under the conditions that are effective during the process of data acquisition. The results discussed in this paper are in good compliance with the claims of [11], and is an important contribution to the related literature.

This paper is organized as follows: The second section presents briefly the SVD technique and its relevance to the modeling strategy. In the third section, development of the reduced order model for the heat conduction phenomenon is analyzed and the infinite dimensional solution of the problem is described. The fourth section presents the simulation results and the concluding remarks are given at the end of the paper.

2. SINGULAR VALUE DECOMPOSITION

Consider the snapshot $d^{(t_h)} = (u(0, t_h), u(\Delta x, t_h), \ldots, u(N\Delta x, t_h))$, which is the data $(u(\cdot, t_h))$ observed from a process at time $t = t_h$. If the data is recorded over a grid having S time points and $N + 1$ spatial locations, the ensemble, D, will be a matrix of dimensions $S \times (N + 1)$; and $d^{(t_h)}$ will be a row of D (or a snapshot from the process) for the observation at time $t = t_h$. Singular value decomposition separates the content of D as follows:

$$D = U\Lambda V^{\mathrm{T}}, \tag{1}$$

where $^{\mathrm{T}}$ denotes the transpose. In Equation (1), U is an $S \times S$ orthogonal matrix, Λ is an $S \times (N + 1)$ matrix containing the singular values in the diagonal with rest of the entries being equal to zero, and V is an $(N + 1) \times (N + 1)$ orthogonal matrix. The first $N + 1$ rows of Λ contain the singular values in decreasing order, that is, $\sigma_1 \geq \sigma_2 \geq \cdots \geq \sigma_{N+1}$.

Defining $Z := U\Lambda$ lets us rewrite Equation (1) as follows

$$D = \sum_{k=1}^{N+1} z_k v_k^{\mathrm{T}}, \tag{2}$$

where z_k and v_k correspond to the kth columns of the matrices Z and V respectively. The representation in Equation (2) contains the full set of modes existing in the ensemble D, if however the expansion is performed utilizing M modes, where $M < N + 1$, one can obtain an approximate reconstruction of the information content of D; and Equation (2) can be rewritten as $D \approx \sum_{k=1}^{M} z_k v_k^{\mathrm{T}}$. The accuracy of this representation is given by the percent energy captured. This measure is described as $E = 100 \left(\sum_{k=1}^{M} \sigma_k \right) / \left(\sum_{k=1}^{N+1} \sigma_k \right)$. The most useful aspect of the representation in Equation (2) is the fact that it contains the temporal information in Z and spatial

information in V. Therefore, one can set desired energy percentage (E), find the necessary number of modes (M) and identify the corresponding columns of Z and V to obtain a reduced order solution given below:

$$u(x,t) \approx \sum_{k=1}^{M} \alpha_k(t)\Phi_k(x), \tag{3}$$

where $\alpha_k(t)$ is a function of time, whose value at time $t = i\Delta t$ is equal to the value seen in the ith entry of z_k. Similarly, $\Phi_k(x)$ is a function of x, and it synthesizes the entries seen in v_k^{T} at every spatial grid point, say $x = j\Delta x$. Therefore, one can visualize the relation between the observed data and these new variables as $(D)_{ij} \approx \sum_{k=1}^{M} \alpha_k(i\Delta t)\Phi_k(j\Delta x)$. This representation is useful for modeling purposes due to the orthonormality of the columns of the matrix V. In what follows, obtaining the reduced order models based on the approximation in Equation (3) is discussed.

3. REDUCED ORDER MODELING OF HEAT CONDUCTION PROCESS

In this section, we apply SVD technique to the one dimensional heat conduction equation described by

$$\frac{\partial u(x,t)}{\partial t} = c^2 \frac{\partial^2 u(x,t)}{\partial x^2}, \tag{4}$$

where $c = c_m + \Delta c$ is the thermal diffusivity parameter with known nominal value c_m and constant uncertainty denoted by Δc. The initial and boundary conditions are specified as follows: $u(x,0) = 0$ for $\forall x$, $u(0,t) = \gamma_0(t)$ and $u(1,t) = \gamma_1(t)$ where $\gamma_0(t)$ and $\gamma_1(t)$ are the external inputs of the system.

Let $\mathcal{C}$ be a class of signals defined as $\mathcal{C} = \{g_k = W_L h : h \in \mathcal{L}_\infty, ||h||_\infty \leq 1\}$, W_L is a lowpass filter with cutoff frequency f_c (Hz) and k is 0 or 1. Denote the solution $u^{\{0\}}(x,t)$ observed when $\gamma_0(t) = g_0(t)$ and $\gamma_1(t) = 0$, and denote the solution $u^{\{1\}}(x,t)$ observed when $\gamma_0(t) = 0$ and $\gamma_1(t) = g_1(t)$. The superscripts $\{0\}$ and $\{1\}$ refer to the variables relevant to the boundary conditions $\gamma_0(t)$ and $\gamma_1(t)$ respectively, and $g_0(t) \in \mathcal{C}$ and $g_1(t) \in \mathcal{C}$ are the arbitrarily chosen test signals. Under these conditions, it should be clear that $u(x,t) = u^{\{0\}}(x,t) + u^{\{1\}}(x,t)$ would be the solution of the PDE in Equation (4) and the boundary conditions leading to this solution would be $\gamma_0(t) = g_0(t)$ and $\gamma_1(t) = g_1(t)$. Since the SVD scheme yields the decomposition

$$u(x,t) = \sum_{i=1}^{M} (\alpha_i^{\{0\}}(t)\Phi_i^{\{0\}}(x) + \alpha_i^{\{1\}}(t)\Phi_i^{\{1\}}(x)), \tag{5}$$

inserting this into Equation (4) results in

$$\sum_{i=1}^{M} (\dot{\alpha}_i^{\{0\}}(t)\Phi_i^{\{0\}}(x) + \dot{\alpha}_i^{\{1\}}(t)\Phi_i^{\{1\}}(x))$$

$$= c^2 \sum_{i=1}^{M} \left(\alpha_i^{\{0\}}(t) \frac{\partial^2 \Phi_i^{\{0\}}(x)}{\partial x^2} + \alpha_i^{\{1\}}(t) \frac{\partial^2 \Phi_i^{\{1\}}(x)}{\partial x^2} \right). \tag{6}$$

Clearly, determining a useful set of basis functions from Equation (6) is very difficult if both of the boundary conditions are arbitrarily chosen functions from $\mathcal{C}$. For this purpose, one can separate the terms in Equation (6) as follows:

$$\sum_{i=1}^{M} \dot{\alpha}_i^{\{0\}}(t)\Phi_i^{\{0\}}(x) = c^2 \sum_{i=1}^{M} \alpha_i^{\{0\}}(t) \frac{\partial^2 \Phi_i^{\{0\}}(x)}{\partial x^2}, \tag{7}$$

which is obtained when $\gamma_1(t) = 0$ and $\gamma_0(t) \in \mathcal{C}$. Similarly,

$$\sum_{i=1}^{M} \dot{\alpha}_i^{\{1\}}(t)\Phi_i^{\{1\}}(x) = c^2 \sum_{i=1}^{M} \alpha_i^{\{1\}}(t) \frac{\partial^2 \Phi_i^{\{1\}}(x)}{\partial x^2}, \tag{8}$$

which is obtained when $\gamma_0(t) = 0$ and $\gamma_1(t) \in \mathcal{C}$. The useful fact here is that the basis functions seen in Equations (7) and (8) are those seen in Equation (6). Therefore, to extract the effect of each individual boundary condition, we will analyze the spatial effects of the chosen boundary condition by holding the other input at zero. For this purpose, consider the case $\gamma_0(t) = 0$ and $\gamma_1(t) \in \mathcal{C}$. This will let us postulate the dynamical system responding to the stimulus at $x = 1$. Since $\gamma_0(t) = 0$, the SVD scheme gives the approximate solution in the following form:

$$u(x,t) = u^{\{1\}}(x,t) = \sum_{i=1}^{M} \alpha_i^{\{1\}}(t)\Phi_i^{\{1\}}(x), \tag{9}$$

which has to satisfy the PDE in Equation (4). Inserting Equation (9) into Equation (4) yields the following relation

$$\sum_{i=1}^{M} \dot{\alpha}_i^{\{1\}}(t)\Phi_i^{\{1\}}(x) = (c_m^2 + c_\Delta) \sum_{i=1}^{M} \alpha_i^{\{1\}}(t)\xi_i^{\{1\}}(x), \tag{10}$$

where $\xi_i^{\{1\}}(x) = \partial^2 \Phi_i^{\{1\}}(x)/\partial x^2$ and $c_\Delta = 2c_m(\Delta c) + (\Delta c)^2$. Knowing that

$$\langle \Phi_i^{\{1\}}(x), \Phi_j^{\{1\}}(x) \rangle = \delta_{ij} = \begin{cases} 1, & \text{if } i = j \\ 0, & \text{otherwise} \end{cases},$$

and taking the inner product of both sides of Equation (10) with $\Phi_k^{\{1\}}(x)$, which corresponds to the Galerkin projection, result in the equality in Equation (11)

$$\dot{\alpha}_k^{\{1\}}(t) = (c_m^2 + c_\Delta) \sum_{i=1}^{M} \alpha_i^{\{1\}}(t) \langle \Phi_k^{\{1\}}(x), \xi_i^{\{1\}}(x) \rangle. \tag{11}$$

As mentioned earlier, the effects of the external stimuli are implicit in the above equation. For this reason, define the grid as $\underline{x} = \bigcup_{i=0}^{N} i(\Delta x)$, where Δx is the spatial step size and $N + 1$ is the number of grid points considered for the numerical solution satisfying $N\Delta x = 1$. Partitioning the grid as $\underline{x} = 0 \cup (\bigcup_{i=1}^{N-1} i(\Delta x)) \cup 1 = (0 \ \underline{x}^{\circ T} \ 1)^T$, one can calculate the values of the functions $\Phi_k^{\{1\}}(x)$ and $\xi_i^{\{1\}}(x)$ at every grid point, and rewrite them in the vector form as $\Phi_k^{\{1\}}(\underline{x})$ and $\xi_i^{\{1\}}(\underline{x})$, respectively. Then the inner product of the two functions becomes $\langle f(x), g(x) \rangle = f(\underline{x})^T g(\underline{x})$. Taking this and the above partitioning into account, and rewriting Equation (11) yield

$$\dot{\alpha}_k^{\{1\}}(t) = (c_m^2 + c_\Delta) \sum_{i=1}^{M} \alpha_i^{\{1\}}(t) \Phi_k^{\{1\}}(\underline{x}^\circ)^T \xi_i^{\{1\}}(\underline{x}^\circ)$$

$$+ (c_m^2 + c_\Delta) \sum_{i=1}^{M} \alpha_i^{\{1\}}(t) \Phi_k^{\{1\}}(0) \xi_i^{\{1\}}(0)$$

$$+ (c_m^2 + c_\Delta) \sum_{i=1}^{M} \alpha_i^{\{1\}}(t) \Phi_k^{\{1\}}(1) \xi_i^{\{1\}}(1). \tag{12}$$

One should notice that although we are examining the dynamics caused by the stimulus at $x = 1$, the above expansion treats the quantities relevant to $x = 0$ separately. This is required because in realistic test conditions, both inputs may assume nonzero values and the effects of them must perfectly be separated to observe a good match between the approximate solution and the numerical solution.

An important observation on Equation (11) is that the external inputs are not seen explicitly. In what follows, the terms in Equation (12) will be manipulated such that the two dynamics are separated properly. The first one is specified independently at the boundaries, while the second one is determined by the governing PDE, that is, Equation (4). The information over the physical domain of the latter is not specified independently. The driving point is to notice that the solution in Equation (9) must be satisfied at the boundaries as well. This gives the following information;

$$u(1, t) = u^{\{1\}}(1, t) = \gamma_1(t) = \sum_{i=1}^{M} \alpha_i^{\{1\}}(t) \Phi_i^{\{1\}}(1), \quad \forall t \geq 0. \tag{13}$$

Or equivalently,

$$\alpha_k^{\{1\}}(t) \Phi_k^{\{1\}}(1) \xi_k^{\{1\}}(1) = \gamma_1(t) \xi_k^{\{1\}}(1) - \sum_{i=1}^{M} (1 - \delta_{ik}) \alpha_i^{\{1\}}(t) \Phi_i^{\{1\}}(1) \xi_k^{\{1\}}(1). \tag{14}$$

In a similar fashion, for $x = 0$, we have the following equality:

$$u(0,t) = u^{\{1\}}(0,t) = \gamma_0(t) = 0 = \sum_{i=1}^{M} \alpha_i^{\{1\}}(t)\Phi_i^{\{1\}}(0), \quad \forall t \geq 0. \tag{15}$$

Or equivalently,

$$\alpha_k^{\{1\}}(t)\Phi_k^{\{1\}}(0)\xi_k^{\{1\}}(0) = \gamma_0(t)\xi_k^{\{1\}}(0) - \sum_{i=1}^{M}(1-\delta_{ik})\alpha_i^{\{1\}}(t)\Phi_i^{\{1\}}(0)\xi_k^{\{1\}}(0). \tag{16}$$

Apparently since $\gamma_0(t) = 0$, the relevant term can be eliminated. However, for nonzero boundary conditions at both inputs, this term introduces the cross interaction. Therefore, due to – probably nonzero – gain $\xi_k^{\{1\}}(0)$ of $\gamma_0(t)$, the term should not be deleted.

Now, we will analyze the last two terms of Equation (12) by utilizing Equations (14) and (16). Firstly, rewrite the summation of the second term in Equation (12) as follows and insert Equation (16) into the result. This gives the second line of Equation (17).

$$\sum_{i=1}^{M} \alpha_i^{\{1\}}(t)\Phi_k^{\{1\}}(0)\xi_i^{\{1\}}(0)$$

$$= \alpha_k^{\{1\}}(t)\Phi_k^{\{1\}}(0)\xi_k^{\{1\}}(0) + \sum_{i=1}^{M}(1-\delta_{ik})\alpha_i^{\{1\}}(t)\Phi_k^{\{1\}}(0)\xi_i^{\{1\}}(0)$$

$$= \gamma_0(t)\xi_k^{\{1\}}(0) - \sum_{i=1}^{M} \alpha_i^{\{1\}}(t)(\Phi_i^{\{1\}}(0)\xi_k^{\{1\}}(0) - \Phi_k^{\{1\}}(0)\xi_i^{\{1\}}(0)) \tag{17}$$

The same rearrangement for the last summation in Equation (12) by using Equation (14) yields

$$\sum_{i=1}^{M} \alpha_i^{\{1\}}(t)\Phi_k^{\{1\}}(1)\xi_i^{\{1\}}(1)$$

$$= \alpha_k^{\{1\}}(t)\Phi_k^{\{1\}}(1)\xi_k^{\{1\}}(1) + \sum_{i=1}^{M}(1-\delta_{ik})\alpha_i^{\{1\}}(t)\Phi_k^{\{1\}}(1)\xi_i^{\{1\}}(1)$$

$$= \gamma_1(t)\xi_k^{\{1\}}(1) - \sum_{i=1}^{M} \alpha_i^{\{1\}}(t)(\Phi_i^{\{1\}}(1)\xi_k^{\{1\}}(1) - \Phi_k^{\{1\}}(1)\xi_i^{\{1\}}(1)) \tag{18}$$

Concatenate all three terms in Equation (12), using Equations (17) and (18) and defining the state vector as $\underline{\alpha}^{\{1\}} = (\alpha_1^{\{1\}}\alpha_2^{\{1\}}\ldots\alpha_M^{\{1\}})^{\mathrm{T}}$ yields the following result:

$$\underline{\dot{\alpha}}^{\{1\}}(t) = (A^{\{1\}} + \Delta A^{\{1\}})\underline{\alpha}^{\{1\}}(t) + (B^{\{1\}} + \Delta B^{\{1\}})\underline{\gamma}(t), \quad \text{with } \underline{\alpha}^{\{1\}}(0) = \underline{0} \tag{19}$$

where $\underline{\gamma}(t) = (\gamma_0(t)\gamma_1(t))^\mathrm{T}$ and

$$[A^{\{1\}}]_{ki} = c_m^2(\Phi_k^{\{1\}}(\underline{x})^\mathrm{T}\xi_i^{\{1\}}(\underline{x}) - \Phi_i^{\{1\}}(0)\xi_k^{\{1\}}(0) - \Phi_i^{\{1\}}(1)\xi_k^{\{1\}}(1))$$

$$[\Delta A^{\{1\}}]_{ki} = c_\Delta(\Phi_k^{\{1\}}(\underline{x})^\mathrm{T}\xi_i^{\{1\}}(\underline{x}) - \Phi_i^{\{1\}}(0)\xi_k^{\{1\}}(0) - \Phi_i^{\{1\}}(1)\xi_k^{\{1\}}(1))$$

$$[B^{\{1\}}]_k = c_m^2(\xi_k^{\{1\}}(0)\ \xi_k^{\{1\}}(1))$$

$$[\Delta B^{\{1\}}]_k = c_\Delta(\xi_k^{\{1\}}(0)\ \xi_k^{\{1\}}(1)). \tag{20}$$

If the procedure described through Equations (9)–(20) is repeated for the case $\gamma_0(t) \in \mathcal{C}$ and $\gamma_1(t) = 0$, it yields

$$\underline{\dot{\alpha}}^{\{0\}}(t) = (A^{\{0\}} + \Delta A^{\{0\}})\underline{\alpha}^{\{0\}}(t) + (B^{\{0\}} + \Delta B^{\{0\}})\underline{\gamma}(t), \quad \text{with } \underline{\alpha}^{\{0\}}(0) = \underline{0} \tag{21}$$

where

$$[A^{\{0\}}]_{ki} = c_m^2(\Phi_k^{\{0\}}(\underline{x})^\mathrm{T}\xi_i^{\{0\}}(\underline{x}) - \Phi_i^{\{0\}}(0)\xi_k^{\{0\}}(0) - \Phi_i^{\{0\}}(1)\xi_k^{\{0\}}(1))$$

$$[\Delta A^{\{0\}}]_{ki} = c_\Delta(\Phi_k^{\{0\}}(\underline{x})^\mathrm{T}\xi_i^{\{0\}}(\underline{x}) - \Phi_i^{\{0\}}(0)\xi_k^{\{0\}}(0) - \Phi_i^{\{0\}}(1)\xi_k^{\{0\}}(1))$$

$$[B^{\{0\}}]_k = c_m^2(\xi_k^{\{0\}}(0)\ \xi_k^{\{0\}}(1))$$

$$[\Delta B^{\{0\}}]_k = c_\Delta(\xi_k^{\{0\}}(0)\ \xi_k^{\{0\}}(1)). \tag{22}$$

At this point, given $\gamma_0(t) = g_0(t)$ and $\gamma_1(t) = g_1(t)$, the dynamical models in Equations (19) and (21) synthesize the temporal components, and the output is calculated as described in Equation (5).

Denoting the Laplace transform operator by $\mathcal{L}\{\bullet\}$ and defining $\mathcal{L}\{u^{\{0\}}(x,t)\} = U^{\{0\}}(x,s), \mathcal{L}\{u^{\{1\}}(x,t)\} = U^{\{1\}}(x,s), \mathcal{L}\{u(0,t)\} = \mathcal{L}\{\gamma_0(t)\} = \Gamma_0(s)$ and $\mathcal{L}\{u(1,t)\} = \mathcal{L}\{\gamma_1(t)\} = \Gamma_1(s)$, a compact representation of the dynamics can be given as follows:

$$\begin{bmatrix} U^{\{0\}}(x,s) \\ U^{\{1\}}(x,s) \end{bmatrix} = \begin{bmatrix} G_{00}(x,s) & G_{01}(x,s) \\ G_{10}(x,s) & G_{11}(x,s) \end{bmatrix} \begin{bmatrix} \Gamma_0(s) \\ \Gamma_1(s) \end{bmatrix} \tag{23}$$

Considering Equation (5), the above representation takes the form below:

$$U(x,s) = (G_{00}(x,s) + G_{10}(x,s))\Gamma_0(s) + (G_{01}(x,s) + G_{11}(x,s))\Gamma_1(s) \tag{24}$$

where $U(x,s) = \mathcal{L}\{u(x,t)\}$. This last representation will let us compare the frequency response of the approximate model and that of the irrational transfer functions, which are discussed next.

The exact solution of Equation (4) with zero initial condition is expressed as

$$U(x,s) = H^{\{0\}}(x,s)\Gamma_0(s) + H^{\{1\}}(x,s)\Gamma_1(s) \tag{25}$$

where

$$H^{\{0\}}(x,s) = \frac{\sinh((\sqrt{s}/c)(1-x))}{\sinh(\sqrt{s}/c)} \qquad (26)$$

and

$$H^{\{1\}}(x,s) = \frac{\sinh((\sqrt{s}/c)x)}{\sinh(\sqrt{s}/c)} \qquad (27)$$

For a thorough investigation of this matter, the reader is referred to [9] and the references therein. In what follows, we present the details concerning the modeling studies with an exemplar case and the comparison of Equations (24) and (25) in frequency domain.

4. SIMULATION STUDIES

For obtaining a set of ODEs characterizing the dominant dynamics, the PDE in Equation (4) has been solved by using Crank-Nicholson method (see [12]) for a set of boundary conditions according to the procedure discussed. The solution has been obtained over a grid possessing equally spaced 100 spatial points, that is, $N + 1 = 100$ ($\Delta x = 1/99$), and the time interval (Δt) has been chosen as 1 msec ($S = 1001$). As the test inputs, we have considered $g(t) = 1$, $g(t) = t$, $g(t) = 1 - \exp(-6t)$ and $g(t) = \sin(2\pi t)$ while applying these from one end and holding the other end at zero. One should note that by choosing these boundary conditions, which are similar to each other in frequency content, the frequency range up to $f_c \approx 10\,\mathrm{Hz}$ over which the model is to be valid is specified indirectly. In this paper, these are the cases we are interested in, and the result is expected to capture all of them on the implied frequency range. Having obtained the solutions, SVD procedure is applied for each case. We have observed that keeping five modes ($M = 5$) captured in average 99.9459% of the total energy described in the second section.

In the simulations, the components of the thermal diffusivity parameter are taken as $c_m = 1$ and $\Delta c = 0.05$. The obtained basis functions have been used to calculate the terms in Equations (20) and (22), which are the system matrices and uncertainty terms. In Figure 1, modeling results for an exemplar case are illustrated. The chosen boundary conditions are $\gamma_0(t) = \mathrm{sgn}(\sin(4\pi t))$ and $\gamma_1(t) = \cos(\pi t)\cos(10\pi t)$, the frequency domain pictures of which are similar to the model derivation conditions. Despite the excitement of slightly higher frequencies due to $\mathrm{sgn}(\cdot)$ function and $\cos(10\pi t)$ term, the figure clearly emphasizes a very good match in space-time domain. In Figure 2, the comparison of frequency domain pictures is presented. For this purpose, define

$$G^{\{0\}}(x,s) = G_{00}(x,s) + G_{10}(x,s), \quad \text{and} \quad G^{\{1\}}(x,s) = G_{01}(x,s) + G_{11}(x,s). \qquad (28)$$
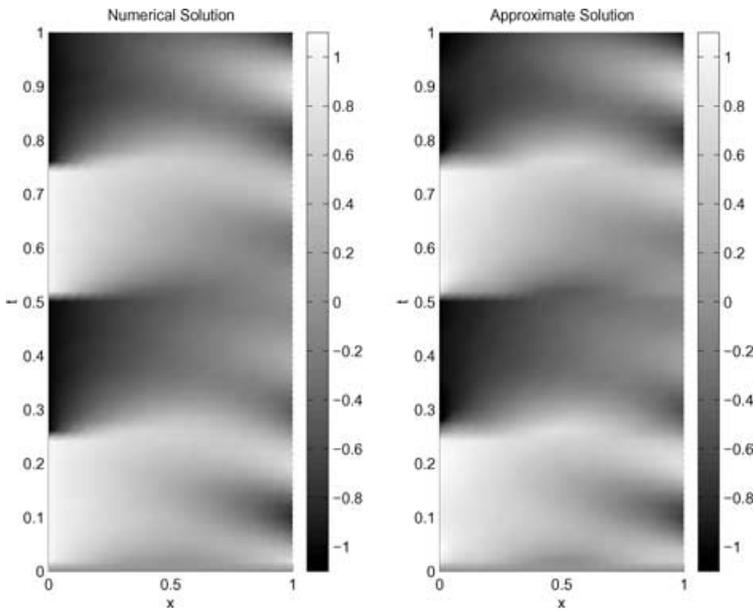
Fig. 1. A comparison of the numerical solution and approximate solution when $\gamma_0(t) = \mathrm{sgn}(\sin(4\pi t))$ and $\gamma_1(t) = \cos(\pi t)\cos(10\pi t)$.

In upper left and upper right subplots of Figure 2, $|H^{\{0\}}(x,j\omega)|$ and $|H^{\{1\}}(x,j\omega)|$ are plotted respectively. The lower left and lower right subplots illustrate what have been obtained through SVD based approximate modeling, that is, $|G^{\{0\}}(x,j\omega)|$ and $|G^{\{1\}}(x,j\omega)|$ respectively. Clearly, if one compares the results seen on each column of the figure, it becomes evident that the approximate model is able to reconstruct the space-frequency picture of the infinite dimensional transfer functions over the range of interest. As depicted in Figure 2, the finite dimensional approximation exhibits discrepancies from the infinite dimensional model. Under the conditions studied, the mismatch seen there is not removable due to the facts discussed in the sequel.

Figure 3 depicts the quantities $|H^{\{0\}}(x,j\omega) - G^{\{0\}}(x,j\omega)|$, which is on the left subplot, and $|H^{\{1\}}(x,j\omega) - G^{\{1\}}(x,j\omega)|$, which is on the right subplot. The surfaces indicate that the approximation is good approximately up to 10 Hz. It is not surprising to get symmetric error plots but one fact needs emphasis: The models in Equations (19) and (21) perform better around the middle of the physical domain than the locations close to the boundaries. Particularly, the model in Equation (19) reveals the best match when $x \approx 0.31$ (refer to the right subplot) and the model in Equation (21) does when $x \approx 0.69$ as seen in the left subplot. Although the points of best match
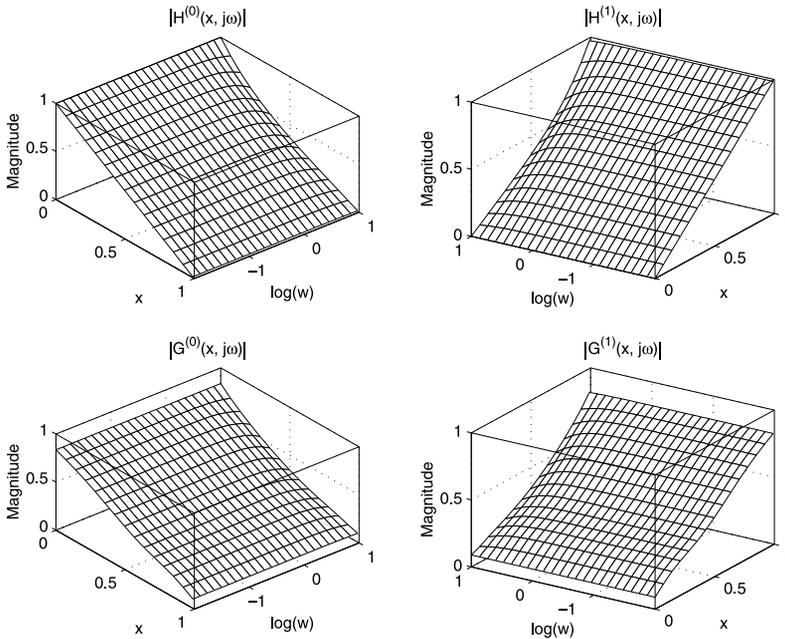
Fig. 2. A comparison of the magnitudes of infinite dimensional transfer functions $[(H^{\{0\}}(x,j\omega)$ and $H^{\{1\}}(x,j\omega))$ and transfer functions based on approximate model $(G^{\{0\}}(x,j\omega)$ and $G^{\{1\}}(x,j\omega))]$.

move slightly with increasing frequency, the error surfaces indicate that a stationary error behavior is obtained over the considered frequency range.

Considering the results presented through the figures, if the signals applied from the boundaries are not from $\mathcal{C}$, the approximation accuracy decreases inevitably. The reason for this is the lack of relevant data in the model derivation stage. If a better accuracy at high frequencies is sought, one has to increase M, the number of modes included and choose excitation signals that are richer in frequency content. However, since the less effective modes contain small-in-magnitude but high-in-frequency information, calculation of the spatial derivatives ($\xi(x)$) contain higher uncertainties and one needs to increase spatial resolution by increasing N. As a result of this, to obtain same level of accuracy on the solution, setting a lowered simulation stepsize (Δt) will be needed inevitably. Apparently, the ultimate cost of improving the accuracy for relatively-higher frequencies will be to give concessions from computational complexity. In the view of all these, one should understand the underlying trade-off between the model simplicity and better matching of the frequency responses. From this point of view, the mismatch around $x = 0$ and $x = 1$ is an expected result and it seems tolerable when considered with the result in Figure 1.
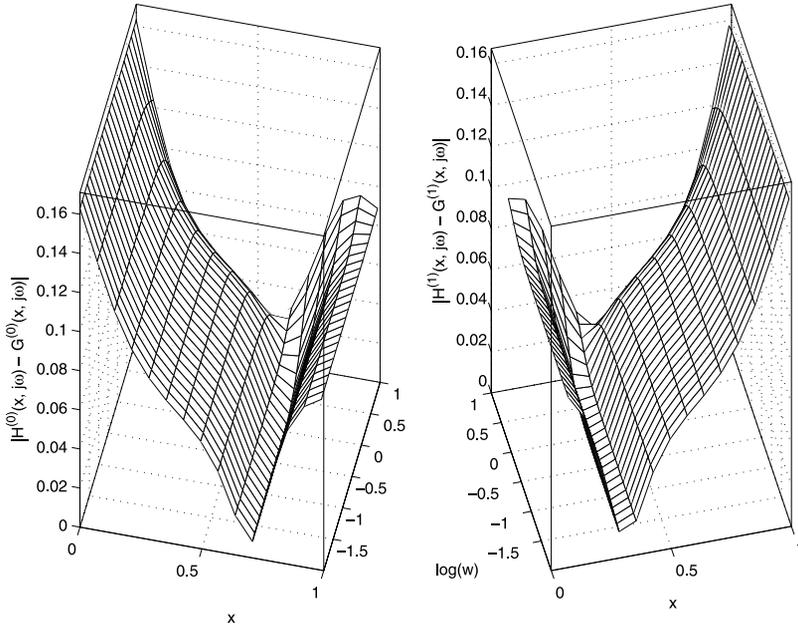
Fig. 3. Reconstruction error magnitudes: $|H^{\{0\}}(x,j\omega) - G^{\{0\}}(x,j\omega)|$ on the left, and $|H^{\{1\}}(x,j\omega) - G^{\{1\}}(x,j\omega)|$ on the right.

Furthermore, one has to notice that since the goal is to find a reduced order model, observing such high-frequency mismatches should not be surprising.

Our work has also proved that the approximate model can further be simplified. We have examined the poles and the corresponding residues of the partial fraction expansion of the nominal dynamics obtained from Equation (23) in the following form:

$$G_{ij}(x,s) = \sum_{k=1}^{M} \frac{\rho_k(x)}{s + p_k}$$

$$= \frac{\rho_d(x)}{s + p_d} + \sum_{k=1}^{M}(1 - \delta_{kd})\frac{\rho_k(x)}{s + p_k}$$

$$= \frac{\rho_d(x)}{s + p_d} + \Delta G_{ij}(x,s),\qquad(29)$$

and we have determined that a single pole (p_d) associated with the residue ($\rho_d(x)$) is dominating the solution in response to signals from $\mathcal{C}$ as the residues of the remaining poles are observed to be small enough. Then we separated the dominant term from the

full transfer function containing the uncertainties. This has enabled us to suggest the following solution as well as the uncertainty terms stemming from the imprecision on the thermal diffusivity parameter and those stemming from the simplification to a first order dynamics compactly.

$$U(x, s) = \frac{11.4263\rho_d(x)}{s + 10.0788}(\Gamma_0(s) + \Gamma_1(s)) + \Delta(x, s), \tag{30}$$

where $|\Delta(x, s)|_{s=j\omega} < 1.2|\Gamma_0(s) + \Gamma_1(s)|_{s=j\omega}|F(s)|_{s=j\omega}$ and $F(s) = 1/(s/24 + 1)$. In Equation (30), $\rho_d(x)$ is the x-dependent residue of the dominant pole at $s = -10.0788$. One should notice that $F(s)$ has been chosen according to the maximal values of the uncertainty observed at every x location contained in the grid. Therefore the above bound does not depend on x. This obviously suggests that a controller, for instance a $\mathcal{H}_\infty$ based controller capable of rejecting the modeling errors, can be designed to observe a predefined thermal behavior at any spatial location. Needless to say, since the low dimensional model is valid up to $f_c \approx 10\,\mathrm{Hz}$ range, the output of a controller has to lie in this frequency region.

5. CONCLUSIONS

Single dimensional heat conduction problem is studied in this paper. The conduction domain is assumed to have uncertain thermal diffusivity parameter. The numerical solution has been obtained by utilizing Crank–Nicholson method, and the spatial and temporal components have been decomposed by SVD technique. The terms in the expansion have been separated so as to observe the boundary conditions as the external inputs. Several test cases have been considered to obtain the dynamic system producing the temporal modes. These efforts have resulted in the nominal dynamics and the uncertainty component due to the imprecisely known process parameter. The results produced by the approximating dynamical model and the numerical solution have been demonstrated to be very similar. Infinite dimensional representation has been generated and the similarity between the frequency responses of the analytic solution and the approximate solution has been proved. It is emphasized that in order to observe a good match, the model-derivation conditions and test conditions must be compatible in frequency domain. It has also been discussed that the uncertainties are bounded and with several simplifications, the design of a thermal control system is fairly simple. The contribution of the paper is to show how SVD (or POD) scheme can be manipulated to separate the control terms and how the uncertainties are characterized in such a modeling problem.

One important aspect of decomposition based approaches is that the methods SVD or POD yield locally valid models. In other words, every model is valid under the operating conditions that enable the synthesis of it. Since the input to the procedure is a set of

snapshots, the dynamical content of the models become limited with what the snapshots imply.

Our work in this field has also demonstrated that without changing anything, the technique to separate external excitations presented in this paper is applicable to nonlinear PDEs particularly for Navier-Stokes equations. Our future study aims to validate those in real-time flow modeling applications.

ACKNOWLEDGEMENTS

REFERENCES

1. Ravindran, S.S.: A Reduced Order Approach for Optimal Control of Fluids Using Proper Orthogonal Decomposition. *Int. J. Num. Meth. Fl.* 34 (2000), pp. 425–488.
2. Ly, H.V. and Tran, H.T.: Modeling and Control of Physical Processes Using Proper Orthogonal Decomposition. *Math. Comp. Model. Dyn. Syst.* 33 (2001), pp. 223–236.
3. Singh, S.N., Myatt, J.H., Addington, G.A., Banda, S. and Hall, J.K.: Optimal Feedback Control of Vortex Shedding Using Proper Orthogonal Decomposition Models. *Trans. ASME: J. Fluid. Eng.* 123 (2001), pp. 612–618.
4. Blossey, P.N. and Lumley, J.L.: Reduced-Order Modeling and Control of Near-Wall Turbulent Flow. In: *Proceedings of the 38th Conference on Decision and Control.* Phoenix, Arizona, USA, 1999, pp. 2851–2856.
5. Atwell, J.A. and King, B.B.: Proper Orthogonal Decomposition for Reduced Basis Feedback Controllers for Parabolic Equations. *Math. Comp. Model. Dyn. Syst.* 33 (2001), pp. 1–19.
6. Atwell, J.A. and King, B.B.: Computational Aspects of Reduced Basis Feedback Controllers for Spatially Distributed Systems. In: *Proceedings of the 38th Conference on Decision and Control.* Phoenix, Arizona, USA, 1999, pp. 4301–4306.
7. Mizel, V.J. and Seidman, T.I.: An Abstract Bang–Bang Principle and Time-Optimal Boundary Control of the Heat Equation. *SIAM J. Cont. Optim.* 35 (4) (1997), pp. 1204–1216.
8. Rösch, A.: Identification of Nonlinear Heat Transfer Laws by Optimal Control. *Num. Funct. Anal. Optim.* 15 (3–4) (1994), pp. 417–434.
9. Curtain, R.F. and Zwart, H.J.: *An Introduction to Infinite-Dimensional Linear Systems Theory.* Springer-Verlag, New York, 1995, pp. 184–189.
10. Efe, M.Ö. and Özbay, H.: Integral Action Based Dirichlet Boundary Control of Burgers Equation. In: *Proceedings of IEEE International Conference on Control Applications* (*CCA'2003*). Istanbul, Turkey, June 23–25, 2003, pp. 1267–1272.
11. Efe, M.Ö. and Özbay, H.: Proper Orthogonal Decomposition for Reduced Order Modeling: 2D Heat Flow. In: *Proceedings of IEEE International Conference on Control Applications* (*CCA'2003*). Istanbul, Turkey, June 23–25, 2003, pp. 1273–1278.
12. Farlow, S.J.: *Partial Differential Equations for Scientists and Engineers.* Dover Publications Inc., New York, 1993, pp. 317–322.